



HAL
open science

Perovskite solar cells under protons irradiation: From in-situ IV-monitoring to root cause degradation elucidation

Carla Costa, Matthieu Manceau, Sophie Duzellier, Thierry Nuns, Romain Cariou

► To cite this version:

Carla Costa, Matthieu Manceau, Sophie Duzellier, Thierry Nuns, Romain Cariou. Perovskite solar cells under protons irradiation: From in-situ IV-monitoring to root cause degradation elucidation. *Solar Energy Materials and Solar Cells*, 2023, 257, pp.112388. 10.1016/j.solmat.2023.112388. hal-04113919

HAL Id: hal-04113919

<https://hal.science/hal-04113919v1>

Submitted on 1 Jun 2023

HAL is a multi-disciplinary open access archive for the deposit and dissemination of scientific research documents, whether they are published or not. The documents may come from teaching and research institutions in France or abroad, or from public or private research centers.

L'archive ouverte pluridisciplinaire **HAL**, est destinée au dépôt et à la diffusion de documents scientifiques de niveau recherche, publiés ou non, émanant des établissements d'enseignement et de recherche français ou étrangers, des laboratoires publics ou privés.

Perovskite solar cells under protons irradiation: from *in-situ* IV-monitoring to root cause degradation elucidation

Carla Costa^{1,2*}, Matthieu Manceau¹, Sophie Duzellier², Thierry Nuns², Romain Cariou¹

¹Univ. Grenoble Alpes, CEA, Liten, Campus INES, 73375 Le Bourget du Lac, France

²Univ. Toulouse, ONERA, DPHY 31055 Toulouse, France

*carla.costa@cea.fr

Highlights

- *In-situ* IV monitoring of perovskite solar cells under vacuum with 1 MeV protons irradiation
- Determination of an optimum perovskite stoichiometry for radiation hardness & stability: 1.6 eV
- Excellent resistance of perovskite materials until 1×10^{14} protons/cm²
- Cells sub-assemblies irradiations reveal weakness of PTAA hole transport layer at higher fluences

Abstract

In recent years, the mixed halide Perovskite solar cells (PSCs) triggered huge amount of R&D activities, thanks to their excellent optoelectronic properties, fast progressing power conversion efficiencies and low cost potential. On top of that, with their high specific power & compatibility with flexible substrate, PSCs appear as a promising mid/long-term alternative photovoltaic technology for space applications. However, the harsh space environment requires particularly robust PV solutions, especially against electrons & protons irradiations; detailed evaluation and comprehension of ageing under irradiations are thus key steps on PSCs development path. In this paper, we focus on perovskite materials and subsequently solar cells proton radiation hardness, with a fluence up to 5×10^{14} protons/cm² at 1 MeV. Optical, microstructural and electrical characterisations, both *in-situ* and *ex-situ*, are used to track the evolutions of 4 different perovskite stoichiometries under irradiation. To this end, single layers, sub-assemblies and full solar cells stack were exposed to protons flux. This systematic approach allowed us to highlight the differences in radiation hardness of PSCs constituting layers: the photo-active $\text{Cs}_{0.05}\text{FA}_{0.95}\text{Pb}(\text{I}_{1-x}\text{Br}_x)_3$ materials exhibits outstanding radiation hardness under the tested conditions, while the PTAA Hole Transport Layer (HTL) appears as a weak contact layer driving cells performance degradation at high fluences.

Keywords: perovskite, solar cells, space, protons irradiation, *in-situ* characterizations

Introduction

Nowadays, space solar arrays are built on III-V multi-junctions, a solar cell technology that benefits from high & long lasting performances as well as extensive flight heritage [1] [2]. Yet, recently, the strong need for cost reduction in this field has boosted R&D on alternative photovoltaics technologies, such as perovskites solar cells. While perovskites in space would have seemed unrealistic few years ago, today even the idea of manufacturing them on the moon is considered [3]. Looking back at the past 10 years, mixed halide perovskites have aroused increasing interest in the field of photovoltaics because of their excellent optoelectronic properties and low cost potential. Perovskite single junctions have seen their efficiency increase from 3.9% in 2009 [4] to a record 25.5% by 2022 [5] [6]. However, several research and industrial challenges remain before a perovskite photovoltaic technology can power a space mission. While many research groups are working towards increased time stability of PSCs against terrestrial constraints (oxygen, humidity & UV) [7] [8] [9], in space PSCs will be facing

a more severe environment (irradiations, vacuum, temperature, etc.) [10]. We focus in this study on only one of these constraints: proton irradiation at one energy. However, PSCs technology remains appealing for the following reasons:

- Excellent power conversion with $< 1\mu\text{m}$ active material thickness, resulting in high specific power (up to 30 W/g reported) [11],
- Ease of integration on flexible substrates [11] [12] [13],
- Promising resistance to protons [14] [15] [16] [17] & electrons irradiations [14] [18] [19] [20].

In addition, the vacuum encountered in space, though posing other challenges, has the advantage of suppressing humidity exposure in operation (even if humidity would still be present during ground phases). This overall favourable context led several research groups to conduct various flight tests with PSCs. In 2018, I. Cardinaletti *et al.* made the first stratospheric experiment with a balloon reaching 32 km altitude and monitoring J(V) performance of PSCs and others cell technologies for several hours [21]. Two years later, L. K. Reb group have sent a rocket at 200 km altitude with PSCs on board [22]. More recently, in a joint NREL-NASA experiment (MISSE), PSCs were brought to the international space station to study their operation during flight at 415 km orbit, and also post-flight after samples return [23]. Such flight demos are useful to assess the performances of PSCs under relevant combined environment constraints, to build heritage / confidence and to push forward this new technology. However, accelerated ageing studies in ground facilities with a single constraint offer an easier path towards degradation mechanism comprehension, especially given the diversity of materials and processes in use for this emerging photovoltaics branch. Protons irradiations are for instance a key constraints regarding space environment.

To this end, *in-situ* J(V) measurements after proton irradiation have been employed. This original approach allows the direct monitoring of the behaviour of PSCs in conditions close to the space environment (vacuum, AM0 illumination).

The work presented here thus focuses on mixed halide perovskite radiation hardness under 1MeV protons irradiations, with the following sections: i) First, presentation the scope of the work, with the various samples and absorbers investigated, as well as characterization methodology and protons irradiation conditions, ii) the second part deals with the investigation of perovskites optical and microstructural properties before & after irradiations, followed by iii) a study of PSCs performances with *in-situ* J(V) measurements and iv) finally, irradiations performed on selected sub-stack of PSCs, combined with *ex-situ* characterisations are used to identify the origin of the observed degradations.

Materials and methods

Materials

Glass is alkali-free boro-silicate from the Earth industry. PbI_2 (99.99%, trace metal basis, L0279) was purchased from Tokyo Chemical Industry (TCI) and FAI from Greatcells Solar Materials. PbBr_2 (99.999% trace metal basis), CsI (99.999% trace metal basis), N,N-Dimethylformamide (anhydrous, 98.8%), Dimethyl sulfoxide (anhydrous, $\geq 99.9\%$), 4-*tert*-Butylpyridine and Li-TFSI (99.95% trace metal basis) were purchased from Sigma Aldrich. SnO_2 was formulated from an industrial nanoparticle solution and diluted four times in deionized water. PTAA was purchased from EM Index and acetonitrile from Carlo Erba.

Device fabrication

ITO-coated glass substrates (25 x 17 mm²) from Visiontek were cleaned sequentially by a performing ultrasonic treatment in acetone, isopropanol and deionized water for 5 min. A tin (IV) oxide (SnO₂) nanoparticle colloidal suspension with a thickness of 30 nm was spin-coated in 3 steps: 200 rpm for 5 s, 2400 rps for 2 s and 4000 rpm for 40 s on cleaned ITO after UV–ozone treatment for 30 min. The perovskite precursor was prepared in a nitrogen filled glovebox by mixing PbI₂, FAI, PbBr₂ and CsI in a DMF:DMSO (4:1 vol ratio) to obtain a 1.2 M solution with the following formula: Cs_{0.05}FA_{0.95}Pb(I_{1-y}Br_y)₃ with 6% Pb excess and 4 stoichiometries were manufactured with different I/Br ratios: 91/9, 83/17, 75/25 and 67/33. The solution was kept at 40 °C under magnetic stirring overnight. After that, the solution of the perovskite was spin-coated on the SnO₂ using a 3-step spin-coating protocol: 200 rpm for 5 s, 1000 rpm for 10 s and finally 6000 rpm for 20 s. During the final step, 150 μL of chlorobenzene was dropped on the substrate 5 s prior to the end of the protocol. The crystallization was completed by post annealing at 100 °C for 1h in a nitrogen atmosphere for a total thickness of 350 nm for this layer. Finally, PTAA (14 g/L) was also spin-coated at 150 rpm for 40 s and 2000 rpm for 30 s (30 nm). To complete the whole solar cells, 2 different electrodes were used. Some samples were completed with a gold electrode (100 nm) evaporated on top of the HTL layer (S_a = 0.33 cm²) and other samples were completed by ITO electrode (ITO_{Top}) deposited by Physical Vapor Deposition (PVD) without any heat treatment (S_a = 0.5 cm²).

Characterizations

Optical characterization was carried out by a Shimadzu UV-2600 spectrophotometer in the wavelength range of 300 to 1200 nm with an integrating sphere ISR-2600. The measured step height absorbance ratio for the perovskite layers were calculated as the EOL/BOL ratio of the absorbance onset. This jump was calculated for specific wavelengths for each Eg: Eg 1 at 700 and 850 nm ; Eg2 at 680 and 830 nm ; Eg3 at 660 and 810 nm and Eg4 at 640 and 790 nm. Microstructural characterization was carried out using X-ray diffraction (AerisPANalytical, Benchtop X-ray diffractometer) equipped using CoK α radiation source at 40 keV and 15 mA. The angle values were then reported in Cu source which is commonly used in the literature. The ITO peak was taken as a reference on the diffractograms because ITO does not degrade at such fluences. Thus all the intensities measured for the perovskite phase on the different samples were related to the ITO peak for the calculation of the EOL/BOL ratio.

The current density–voltage J(V) curves of solar cells were measured on a Keithley 2402 measure unit under AM1.5G and AM0 illumination at 1000 W m⁻² and 1367 W m⁻² respectively using an Oriel 9403A-SR1 for *ex-situ* measurement and qualified by spectroradiometer. And on a Keithley 4200-SCS under AM0 illumination qualified by III-V cells isotypes for *in-situ* measurement.

TLM measurements was carried out by GP solar “GP4 test” tester and sheet resistance was measured with 4-point probes with a Napson equipment.

SRIM simulation

To simulation depth of defect penetration a total of 1x10⁵ protons were simulated using SRIM. The following material densities were used: $\rho_{\text{ITO}_{\text{Top}}} = 7.2 \text{ g/cm}^3$, $\rho_{\text{PTAA}} = 1.2 \text{ g/cm}^3$, $\rho_{\text{Pk}} = 4.59 \text{ g/cm}^3$, $\rho_{\text{SnO}_2} = 6.85 \text{ g/cm}^3$, $\rho_{\text{ITO}} = 7.2 \text{ g/cm}^3$, $\rho_{\text{glass}} = 2.58 \text{ g/cm}^3$.

Employed particles was : hydrogen, mass = 1.008 amu,
Energy = 1MeV.

Scope of the work

In this study, the performances of un-encapsulated PSCs based on four different perovskite (Pk) compositions are investigated under protons irradiation. It is indeed well known that perovskite bandgap can be adjusted over a rather wide range through stoichiometry tuning [24], and that bandgap (E_g) of cells absorber is a key parameter to reach optimum photovoltaic conversion under a given light spectrum. The Shockley-Queisser (S-Q) limit shows that the optimal gap of a cell for ideal photon collection with AM0 is slightly below 1.3 eV [25] [26]. For PSCs, Z. Yang et al. have shown that the bandgap of a cell is notably controlled by I/Br ratio [27]; thus in order to get close to theoretical E_g optimum, this I/Br ratio was adjusted in the precursors formulation to produce 4 different Pk with general formula $\text{Cs}_{0.05}\text{FA}_{0.95}\text{Pb}(\text{I}_{1-x}\text{Br}_x)_3$ (Eg1, 2, 3 and 4, see Table 1). While the 1.3 eV target could not be reached with the tested perovskite compositions (the tested E_g ranges between 1.57 and 1.68 eV), these four stoichiometries were selected for this study to evaluate performance in both begin-of-life and end-of-life conditions, as well as their intrinsic stability.

$\text{Cs}_{0.05}\text{FA}_{0.95}\text{Pb}(\text{I}_{1-x}\text{Br}_x)_3$		
Label	Ratio I/Br	E_g (eV)
Eg1	91/9	1.57
Eg2	83/17	1.60
Eg3	75/25	1.65
Eg4	67/33	1.68

Table 1. Formulation, I/Br ratios & associated bandgaps for the different perovskite absorbers used in this study

Typically, for III-V solar cells, a complete radiation hardness study for solar cells requires experimental campaigns with protons and electrons irradiations sequences spanning 3 to 12 different energies (JPL or NRL methods)[28]; for protons, the relevant energy range is classically from 0.1 to 10 MeV. Depending on the type of particles and their fluences, it is indeed possible to create very different defects in materials [29]. For emerging thin film technologies such as perovskites, the most relevant irradiation conditions remains the subject of discussions within the community [30] [31]. Indeed, A. R. Kirmani et al. have shown that low energies (e.g. around 50 keV) allowed more displacement damages creation, compared to higher energies (few MeV) where ionization defects are relatively more important. We have therefore chosen in this work to study the effect at 1 MeV, a standard test condition [32]. Indeed, this energy allows a rather homogeneous irradiation of the device layers, i.e. the whole active region ($<1\mu\text{m}$) of the devices sees incident protons with similar energy (very close to 1MeV), unlike in the case of low energy protons. With 1 MeV energy, the protons penetration depth is much smaller than the $500\mu\text{m}$ glass substrate thickness; consequently, protons exposure were performed through the top side of the solar cells (see Figure 1 left). In that case, the protons Bragg peak appears beyond the cells stack ($\sim 15\mu\text{m}$ depth within the glass), as shown in the SRIM simulation [33] in Figure 1, right. Thus, with 1MeV protons irradiation from the top electrode ITO electrode side, defects are created relatively homogeneously through the device layers.

The PSCs in this study were irradiated with a proton beam until a fluence of 5×10^{14} protons/cm². Incremental fluence steps were implemented and *in-situ* J(V) measurements performed at 1×10^{13} , 1×10^{14} and 5×10^{14} protons/cm². The *in-situ* J(V) measurements were performed in a vacuum chamber (MIRAGE at ONERA, Toulouse, France [34]) just after irradiation without breaking vacuum between each step and with thermo-regulation of the sample holder during irradiations and measurements. Details of sample holder, proton flux, beam size and homogeneity are given in Figure S1. These measurement conditions make it

possible to simulate cells operating in conditions close to space environment: it suppresses potential self-healing phenomena that could occur when bringing cells back in air for the measurements [35]. This *in-situ* measurement configuration is also helpful to identify PSCs degradation threshold.

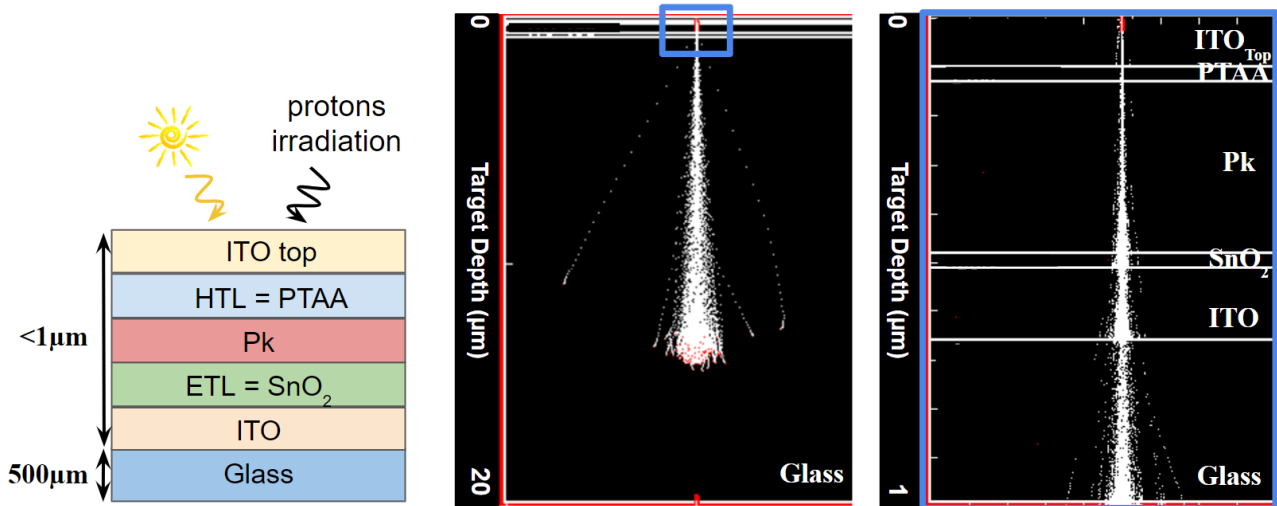


Figure 1. Left: Schematics of perovskite cells stack with irradiation from the top electrode. Right: SRIM simulations of 1 MeV protons trajectories through cells stack showing Bragg peak at 15μm in the glass and a zoom of the top-most 1μm region.

Table 2 summarises all the different stacks and the associated characterisations. All the characterisations were carried out before and after irradiation (Beginning Of Life/ End Of Life: BOL/EOL).

- Stack #1 is used to study the evolution of the optical properties & microstructure BOL/EOL of the perovskite material from UV/Visible Absorbance Spectroscopy and XRD measurements, respectively.
- Stack #2 corresponds to the complete stack of the cell with an ITO (Indium Thin Oxide) top electrode. This transparent electrode is necessary to perform the *in-situ* J(V) measurements within the irradiation chamber (optical port for illumination at a tilted angle with respect to proton beam, (Figure 1, left).
- Stacks #3 and #4 are designed to monitor the evolution of electrical, optical and microstructural properties of the lower and upper electrodes (labelled ITO and ITO_{Top}).
- Stack #5 is focusing on optical properties of the PTAA (Poly-TriAryl-Amine) layer alone, which is the HTL of the cell.
- Stack #6 allowed contact resistivity measurements between the top electrode and the HTL. It compares the PTAA/ITO_{Top} interface used in this study (enabling *in-situ* J(V) measurements) with standard & optimized PTAA/Au interface. For this purpose, TLM (Transmission Line Measurement) resistivity measurements were carried out.
- Stacks #7 and #8 are used to study the degradation of the electrical properties of the Pk and PTAA layers independently of each other. Two incomplete Glass/ITO/SnO₂/Pk and Glass/ITO/SnO₂/Pk/PTAA stacks were irradiated and then completed with the missing contact layers (Au and PTAA/Au respectively).




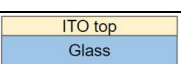
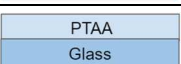

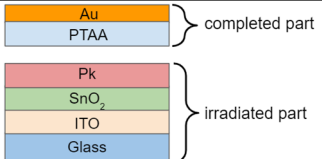
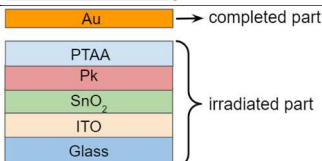
Protons irradiation – 5×10^{14} protons/cm ² @1MeV									
#	Layer stack schematics	Number of (references ; irradiated)	Sheet resistance	Contact resistance	<i>In-situ</i> IV	<i>Ex-situ</i> IV	UV/Vis spectro.	XRD	Objectives
1		(2;4)							BOL & EOL Study of Pk material properties with 4 different bandgaps
2		(NA;6)			BOL & EOL				<i>In-situ</i> study of Pk cells radiation hardness
3		(3;4)		BOL & EOL					Evaluation of contact electrodes radiation hardness
4		(3;4)					BOL & EOL		
5		(2;4)							Study of PTAA single layer radiation hardness
6		(3;4)		BOL & EOL					Study of PTAA/Electrode electrical properties
7		(6;6)							Evaluation of Pk & PTAA layers radiation hardness within PSCs
8		(6;6)							

Table 2. Matrix of samples layer stacks, characterizations steps and objectives.

Results and discussion

1. Perovskite absorber under proton irradiation – material study

Figure 2.a shows UV/Visible Absorption Spectroscopy carried out to study the optical properties of BOL & EOL Pk with various bandgaps (see Table 1). First of all, it is interesting to note that no change in band-gap was observed after application of the Tauc Plot method [36] for all samples before and after storage or irradiation. For a given film thickness and absorption coefficient, in first approximation, the step height scales with the absorber quantity, here the perovskite [37].

Figure 2.b shows the EOL/BOL step height in absorbance for 1 MeV and fluence of 5×10^{14} protons/cm² for the 4 Pk stoichiometries studied (see Table 1). The timescale of these experiments being relatively long (7 days), similar measurements were performed on samples that were stored but not irradiated to distinguish between irradiation and potential storage stability effects (Figure S2). A degradation upon storage for one week under ambient conditions (air & dark) is clearly observed for the most Br-rich series (black curve - Eg4 = 1.68 eV). The origin of the instability of the Br-rich perovskites has already been reported in the literature and would tend to come from Br-induced photo-segregation [38].

Interestingly, a different trend was observed for irradiated samples (red dash curve). While no significant variation is observed for the 3 higher bandgaps perovskites, for the smallest gap (Eg1 = 1.57 eV), a slight absorbance decrease is observed with 10% loss of the absorbance onset. While being closer to the ideal candidate from the efficiency point of view, this suggests that Pk with a high iodine content could be detrimental for irradiation stability. In addition, in different studies, the migration of iodine through the different layers has already been demonstrated with the volatile I₂ present in the Pk layer [15] [39] [40]. It has been shown that this migration can have a negative impact on the electrical properties of the cells. It could be envisaged here that the Eg1 series, which contains a large amount of iodine, similar phenomena could be responsible to the larger degradation observed

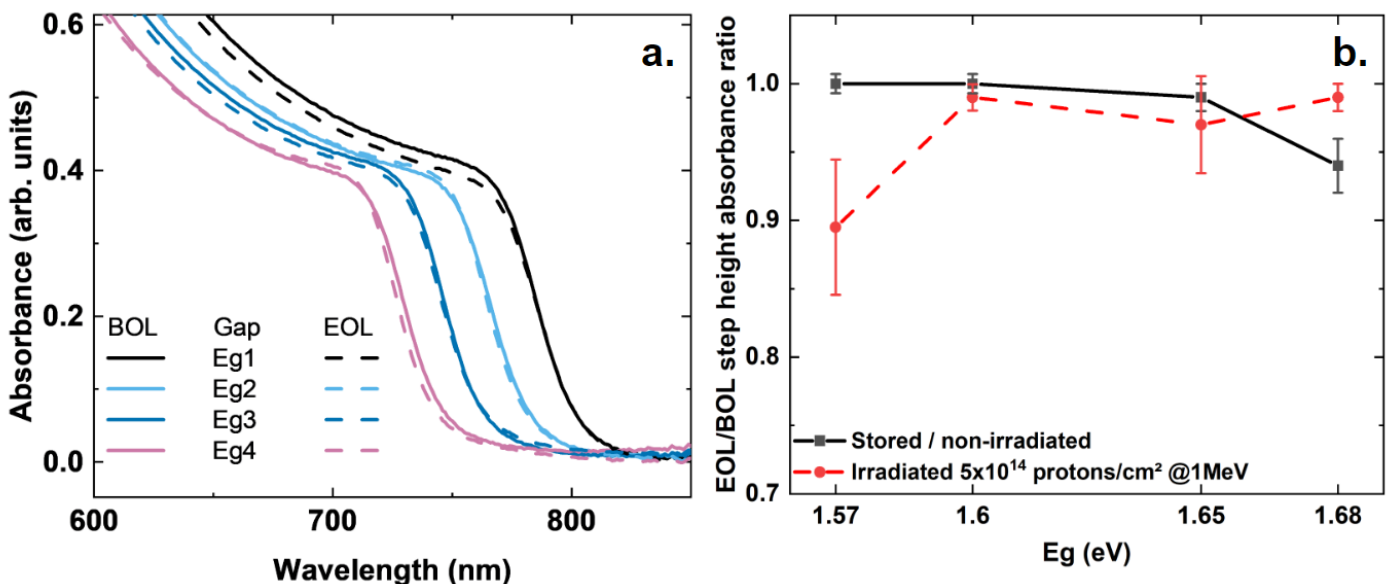


Figure 32.a. UV-vis absorbance spectra for Pk materials (Stack #1, see Table 2- average of 4 samples) before and after 1MeV 5×10^{14} protons/cm² irradiation; b. EOL/BOL absorbance onset for Pk samples (Stack #1, see Table 2) stored in dark & cleanroom (reference - solid line - average of 2 substrates) and after 1MeV 5×10^{14} protons/cm² irradiation (dash line - average of 4 samples) as a function of bandgap.

A study of the Pk microstructure by XRD was also carried out to gain more knowledge about the material behaviour under protons irradiation. Figures 3.a and b show the diffractogram recorded before and after irradiation for the Eg1 and Eg2 series, respectively. It is important to note that the peak associated with the ITO (highlighted by a yellow star) has been taken as a reference. Indeed, the ITO is known to be stable in such irradiation conditions [41]. This peak allows to check if there is a global variation of the signal and thus of the intensity of the diffractogram due to the device. From a general point of view, one can first note on these XRD patterns (see Figure S3 & S4 for Eg3 & Eg4) that protons irradiation did not result in the appearance of new XRD features. More specifically, it is interesting to note that no signature from the δ -phase were detected [42]. As shown in Figure 3.a, the study of the ITO peak reveals an overall signal decrease of $\sim 30\%$. Despite of this diminution, it is also observed a decrease of $\sim 50\%$ of the signal intensity for all the peaks of the α -phase of the perovskite for the Eg1 series. On the contrary, Figure 3.b represents the Eg2 series and shows an increase in the intensity of the perovskite and PbI_2 features. A similar behaviour is observed for the Eg3 and Eg4 series, (see Supports S3 & S4) while the intensity of the ITO peak remains stable. The degradation of Eg1 series coincides with the UV/Visible absorption spectroscopy observations presented above. The increase observed for the other 3 series could come from a higher crystallinity of the Pk material after irradiation. For future works, it will be interesting to realize SEM pictures in order to study the compactness and grain size of Pk layers before and after irradiations. These results are in line with the evolution of the FWHM of the Pk peak (Figure S5). Indeed, one can observe an increase in the FWHM for Eg1 after irradiation corresponding to a decrease in the crystallites size. One can also note the opposite behaviour for the 3 other series: a decrease in FWHM corresponding to an increase in the crystallites size present in the Pk layer. Moreover, it is observed for the stored samples a decrease in Pk peak intensity with increasing Bromine content (Eg3 and 4). This diminution in the amount of crystalline Pk in the layer is also consistent with the UV/Visible Absorption Spectroscopy observations (Figure S6).

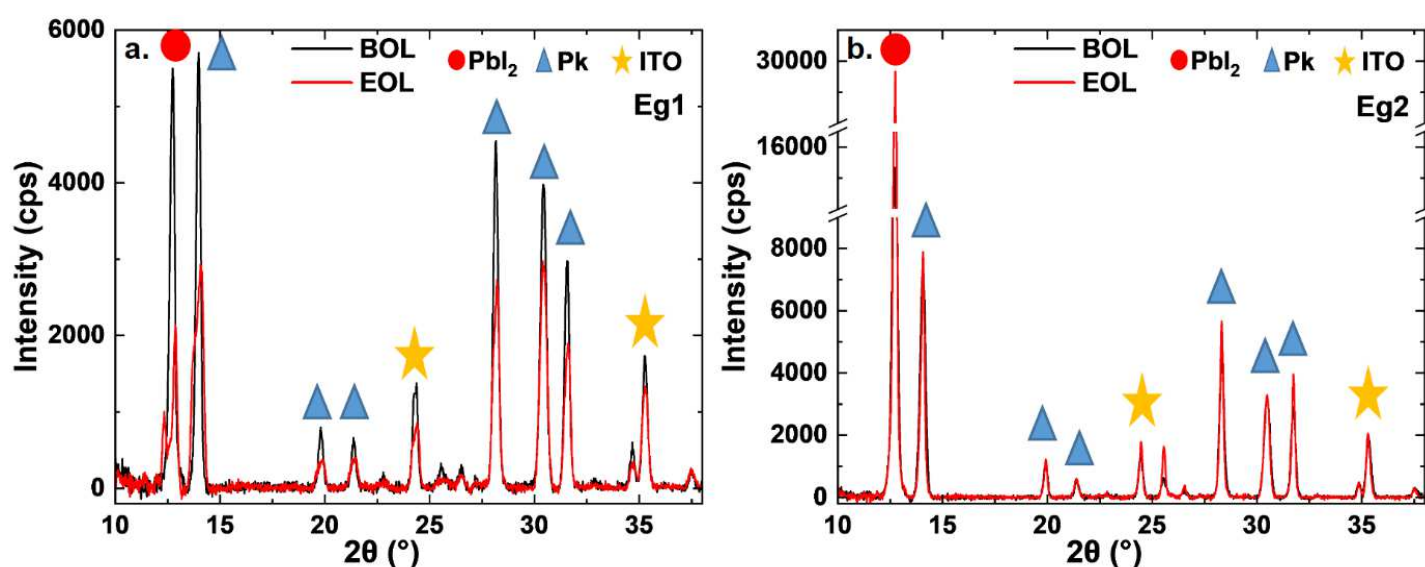


Figure 3. Perovskite samples (Stack #1, see Table 2) diffractograms before and after irradiation with $1 \text{ MeV } 5 \times 10^{14} \text{ protons/cm}^2$ for a. Eg1 series and b. for Eg2 series (see Table 1)

According to this first Pk material characterization, one can conclude that both optical and microstructural properties are not significantly degraded after irradiation at such a high proton fluence, for the three highest bandgap stoichiometries (Eg2, 3 and 4). Conversely, the lowest bandgap (Eg1) samples shows significant degradation under the same conditions. These results are all the more interesting as the reference samples that were stored during the

irradiations do not behave the same way. This highlights both the preponderant degradation of the Br-rich series during storage, as some research groups have already highlighted [32], but also the effect of the Eg on the radiation tolerance. Device efficiency being influenced by a large number of material & layers properties, these observations alone are obviously not sufficient to conclude about device radiation hardness. Yet, maintaining appropriate absorption properties and crystallinity are two prerequisites to get functional devices.

2. *In-situ* J(V) monitoring of PK-based devices

From the previous observations, the photovoltaic behaviour of perovskite-based devices was then monitored *in-situ* in vacuum chamber for each of the 3 steps of irradiations.

2.1 Pre-irradiation testing

As described in the scope of this work, the experimental set-up and the protons irradiations used in this work for *in-situ* J(V) measurements requires cells architectures with transparent top electrodes.

The impact of such a change, compared to state-of-art design with gold contacts, has first been assessed. Typical J(V) curves of devices made with a gold or an ITO_{Top} electrode are shown on Figure 4.a and average device characteristics are grouped in Table 3.

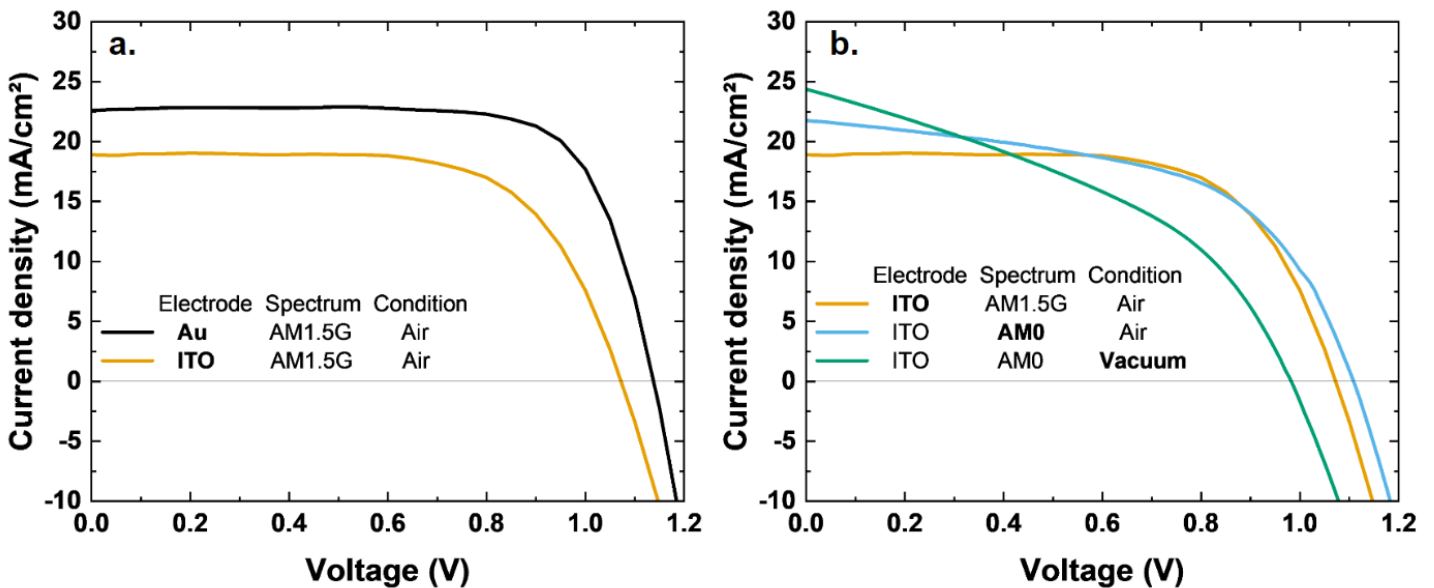


Figure 4.a Influence of contact electrodes materials (Au or ITO) under AM1.5G spectrum, b. Influence of spectra (AM1.5G or AM0) and measurement conditions (Air or Vacuum) on un-encapsulated Pk cells with ITO electrode (Eg2, see Table1).

Top electrode - Spectrum - Atmosphere	Voc (V)	Jsc (mA/cm ²)	FF (%)	PCE (%)
Au - AM1.5G - air	1.139 +/-0.015	22.6 +/-0.2	75 +/-2	19.2 +/-0.7
ITO_{Top} - AM1.5G - air	1.071 +/-0.021	18.9 +/-0.4	67 +/-2	13.6 +/-0.5
ITO_{Top} - AM0 - air	1.109 +/-0.005	22.1 +/-0.8	54 +/-1	9.7 +/-0.6
ITO_{Top} - AM0 - vacuum	0.982 +/-0.014	24.4 +/-1.4	40 +/-3	7.1 +/-0.9

Table 3 - Evolution of Voc, Jsc, FF and PCE for different contact electrodes (Au or ITO_{Top}), spectra (AM1.5G or AM0), and measurement conditions (air or vacuum) for Pk cells (Eg2, see Table1).

The typical efficiency of our reference Pk cells with gold contact under AM1.5G spectrum measured in air is >19%: with Voc = 1.139 V, Jsc = 22.6 mA/cm² and FF = 75%. A significant decrease in efficiency is observed when using an ITO_{Top} electrode (instead of Au) needed for *in-situ* J(V) measurements. This decrease is linked to several combined effects. First, the interface between the polymeric HTL (PTAA) and ITO has not been finely optimised in our process, so FF is impacted as sputter damages from the ITO process has been reported to impair charge extraction [43]. In addition, this ITO electrode is less conductive than Au, which also leads to higher series resistance. Finally, no anti-reflective layer has been added to the ITO which greatly impacts on the Jsc. From these results, it is clear that ITO electrode is not optimal from a device performance point of view; process developments would be required to get similar performances as the gold electrode stack but this goes beyond the scope of this work (e.g. metal oxide buffer layer between PTAA and ITO, anti-reflective coating on top of ITO).

Then, to closely match space PV working conditions, the effects of illumination spectra (AM1.5G & AM0) and measurement conditions (air & vacuum) on PSCs characteristics were evaluated (Fig 4b). When measured under AM0 illumination, the increase of nearly 15% in Jsc is obviously linked to the convolution of the higher AM0 irradiance (1.36x higher than AM1.5G) and the cell spectral response. However, one can see that under AM0, the cell stack with the transparent ITO electrode design is also sub-optimal: significant parasitic resistances lead to FF reduction (67% under AM1.5G versus 54% under AM0). In addition, when measured under vacuum another degradation of Pk cells electrical properties is observed. This deleterious effect under vacuum for un-encapsulated Pk cells has already been documented by several research groups [44] [45]. The observed increase in Jsc (~2 mA/cm²) could reflect an optical change in a layer and/or interface. Complementary analyses (the scope of this paper) such as measurement of the optical properties under vacuum would help to understand this phenomenon. Nonetheless, this effect does not prevent appropriate data analysis, since we perform relative comparison of the cells results with BOL reference being already *in-situ* under vacuum conditions

In light of these results, it is important to stress out that *in-situ* J(V) data will be used for relative comparisons (relative degradation versus fluence steps). Despite the lower initial efficiencies of these devices under AM0 and vacuum conditions, it brings valuable insights on protons-related degradation behaviour.

2.2 Device behaviour under irradiations

Figure 5 shows the evolution of Voc, Jsc, FF and PCE of 6 cells (Stack #2, Table 2) for each of the 4 different stoichiometries which were irradiated at 3 different fluences (1×10^{13} , 1×10^{14} and 5×10^{14} protons/cm²) in order to follow their behaviour under irradiation. The stepwise increase in fluence and the *in-situ* J(V) measurements (without breaking vacuum) made it possible to study the electrical behaviour under irradiation without potential air-related self-healing phenomena [35], this experimental configuration is thus closer to real space conditions. The *in-situ* J(V) measurements for the different steps in fluences highlight:

- Up to 1×10^{13} protons/cm², none of the 4 stoichiometries was further degraded. One can even note a slight efficiency increase that could originate from irradiation induced annealing effect [46]
- From 1×10^{14} protons/cm², degradation starts for the Eg1 series (black square) while the performances of other compositions increase slightly further
- Then, the 4 series clearly degrade from 5×10^{14} protons/cm², with an average loss of 52% of the initial properties. Here again, the FF is largely impacted, this suggests that one of the layers or interfaces of the cell has been degraded.

To sum-up, different degradations pathways can be identified from these *in-situ* measurements. First, measurements under vacuum have shown a clear degradation of the electrical properties. As this is observed for the 4 stoichiometries, this phenomenon could be independent from the perovskite bandgap. Secondly, no degradation is observed for series Eg2, 3 and 4 up to 1×10^{14} protons/cm². Yet, in parallel, a significant degradation of the Voc of Eg1 series is highlighted. A degradation of the open circuit voltage can be directly linked to the intrinsic properties of the layers and this result seems to be in agreement with the degradations observed in the previous section regarding Pk materials properties. This could be explained by the migration of iodine species which are predominantly present in this stoichiometry. The migration of iodine from Pk through the cell layers is widely reported in the literature [47] [48] [49]. Thus, mobile ions I⁻ are likely to be oxidised to iodine I⁰. The latter act as recombination centres and also accelerate the degradation of Pk. Thirdly, a significant degradation of Jsc and FF is observed at 5×10^{14} protons/cm²; this degradation seems to be independent of the Pk stoichiometries as it appears for the four bandgaps.

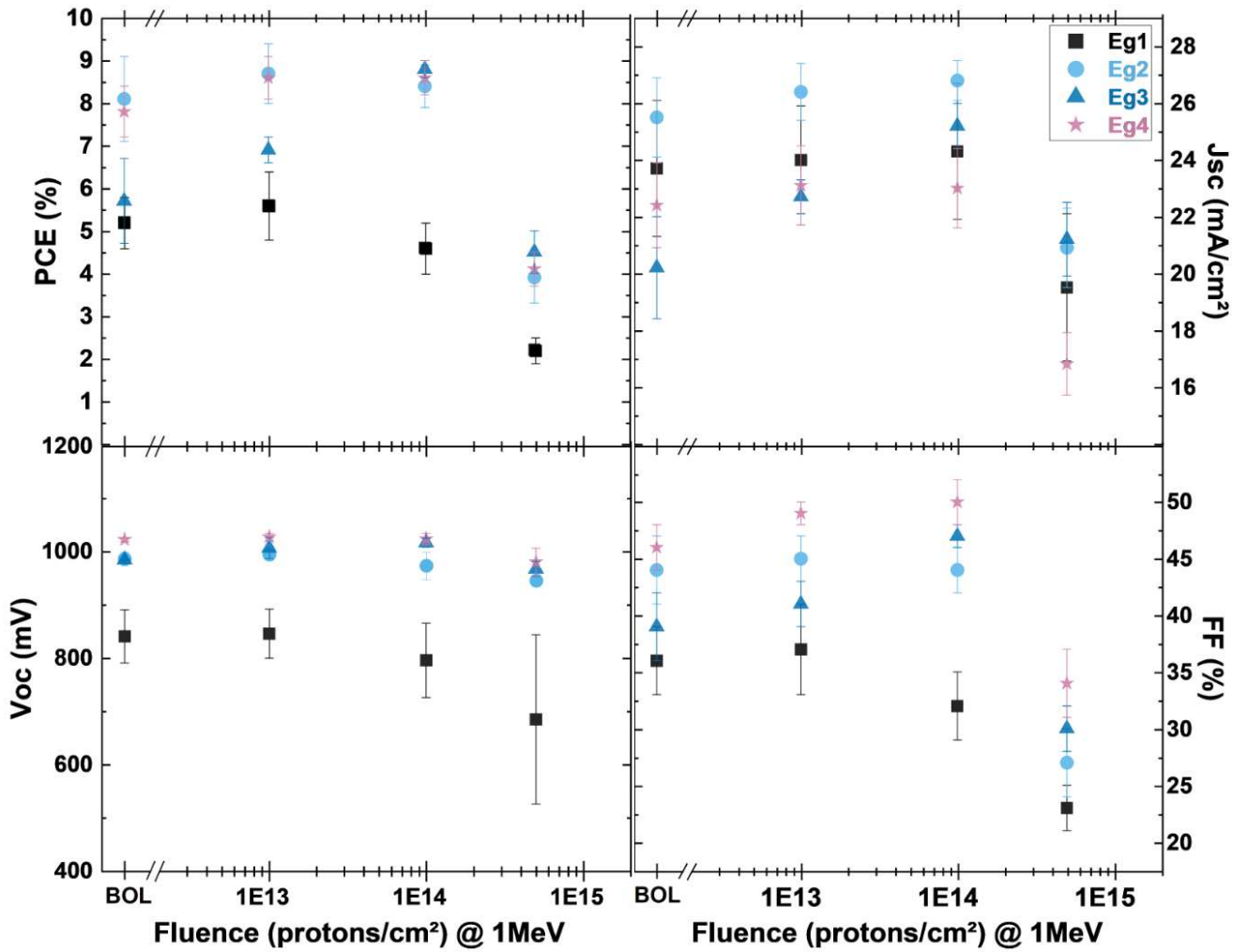


Figure 5. In-situ evolution of PCE, Jsc, Voc and FF with protons irradiations as function of the bandgap (Eg1, Eg2, Eg3 and Eg4, Table 1) for different fluences: 1×10^{13} , 1×10^{14} , 5×10^{14} protons/cm² @ 1MeV under AM0 & vacuum (average of 6 samples)

As documented above, no significant degradation from a material point of view (UV/Vis spectroscopy & XRD) could be detected for the Eg 2, 3 and 4 series up to 5×10^{14} protons/cm². Yet, this does not mean that the electrical properties of these layers are not affected, so further characterisations were therefore necessary to understand the origin of the discrepancy between the Pk radiation hardness (optical and crystalline properties) and device performance degradation (opto-electronic properties). For this purpose, the study of the electrical, optical and microstructural properties of the different layers stack (*i.e.* beyond the absorber) was carried out, before and after irradiations (Stack #3, 4, 5 and 6, see Table 2). In the following, focus will be placed on Eg2 bandgap series and a fluence of 5×10^{14} protons/cm² as this stoichiometry offers good performance and this fluence seems a critical threshold for the investigated PSCs.

3. Root cause degradation analysis

As described before, a significant decrease in J_{sc} & FF is observed for devices at the maximum fluence. As an example of this behaviour, associated $J(V)$ curves of devices from Eg2 series before and after irradiation are presented in Figure 6 (*ex-situ* measurements). From these curves, it is clear that the irradiation leads to a significant increase in series resistance. This behaviour could for instance be linked to the degradation of one of the charge transporting layers (SnO_2 , PTAA) and/or also the degradation of one of the electrodes (ITO & ITO_{Top}). To evaluate the impact of irradiations on these layers, different stacks were irradiated (with $1\text{MeV } 5 \times 10^{14}$ protons/ cm^2).

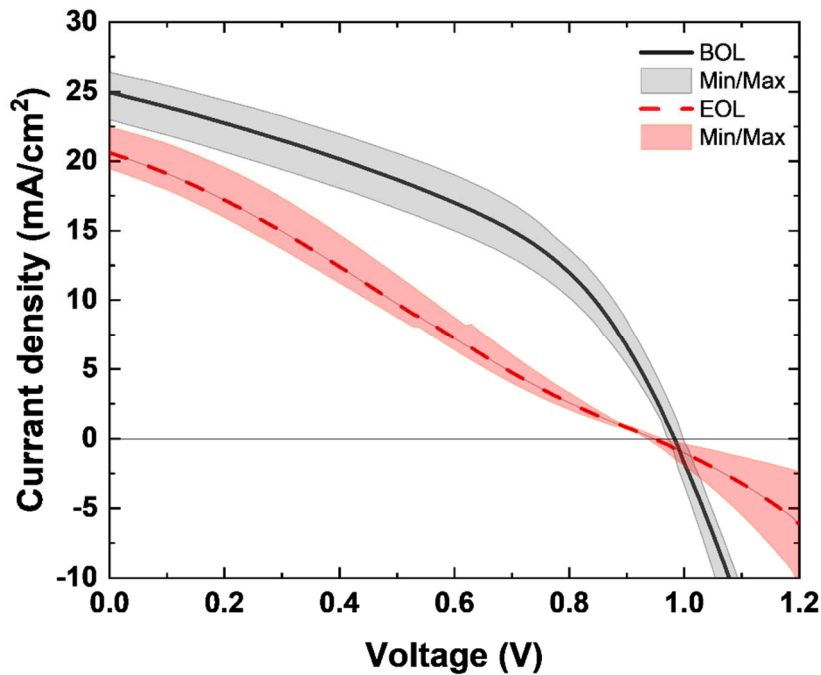


Figure 6. Comparison of JV characteristics for PSCs (Eg2 see Table 1 – Stack #2 see Table 2 – error bar refers to min/max data averaged on 6 samples) before irradiation (BOL - black solid line) and after irradiation (EOL - red dash line) @ $1\text{MeV } 5 \times 10^{14}$ protons/ cm^2 under vacuum and AM0 spectrum.

Stack	Rsheets BOL (Ω/square)	Rsheets EOL (Ω/square)
#3 : Glass/ITO/ SnO_2	8.7 +/-0.1	9.0 +/- 0.1
#4 : Glass/ ITO_{Top}	137.4 +/- 0.1	124.2 +/- 0.1

Table 4. Evolution of sheet resistance for stack #3 and #4 before and after irradiation at 5×10^{14} protons/ cm^2 @ 1MeV

Table 4 summarises the evolution of the R_{sheet} of stacks #3 and #4 before and after irradiation at $1\text{MeV } 5 \times 10^{14}$ protons/ cm^2 . This measurement reveals a slight R_{sheet} increase (< 5%) in the bottom ITO/ SnO_2 stack. Given the device geometry and electrical properties, such an increase in sheet resistance leads to a very moderate increase in the power losses (ca 3%) [50] [51]. It thus cannot justify the FF degradation observed in the *in-situ* $J(V)$ measurements

(35% loss in average). On the same stack, UV-Visible Transmission Spectroscopy and XRD measurements were carried out and showed no degradation of the optical and microstructural properties of the Glass, ITO and SnO₂ layer (Figure S7 & S8).

As for the top electrode (sun facing one, stack#4), sheet resistance measurements showed a decrease about 10% after irradiation. This decrease may be due to a structural rearrangement of the ITO layer caused by energy input during irradiation. It should be noted that during the deposition of this layer, no annealing is carried out in order to avoid potential damage of underneath layers, so this ITO_{Top} layer does not have an optimal structural arrangement and therefore optimal conductive properties. Furthermore, UV/Vis Transmission Spectroscopy measurements on Glass/ITO_{Top} did not reveal any degradation of this layer (Figure S9) ruling out the hypothesis of a decrease in J_{sc} originating from a stronger parasitic absorption and/or higher reflection at the front electrode.

Thus, the two ITO electrodes of the cell are marginally altered by such proton fluence. This is also in good agreement with the work of D. V Morgan *et al* that has shown a remarkable resistance of ITO under protons irradiation, up to fluences of 1×10^{16} protons/cm² [41].

Specific attention was then placed on the PTAA layer. For this purpose, the stack #5 (see Table 2) was irradiated. The BOL/EOL UV/Visible Absorbance Spectroscopy measurements curves are shown in Figure 7. Post-irradiation, an absorbance decrease around 380 nm (from 0.715 A.U. to 0.676 A.U.) is detected. This decrease in absorbance could for instance originate from a reduced conjugation length [52] and hence be the signature of molecular chains scissions. Such a mechanism has already been documented for different conjugated polymers including PTAA under UV light. For instance *M. Petrović et al.* evidenced structural degradation of PTAA that lead to partial decomposition of the conjugated structure [53]. Chain scission under low-energy proton irradiation has already been demonstrated in the past in other polymers such as Polycarbonate Makrofol-De [54]. Moreover, it is interesting to note that in the PTAA molecule the lowest bond energy is the C-N (293 kJ/mol) [55] and the breaking of this bond has also been observed in polyimide-type polymers [56].

Beyond the impact on optical properties, such a degradation could also lead to changes in the electrical properties. *M. Petrović et al* indeed observed that beyond structural integrity, UV exposure increased defect population and hindered hole extraction properties. Other groups have also highlighted the importance of molecular weight, which is directly related to the chain length of PTAA, on solar cell performance. Indeed, the higher the molecular weight, the better the efficiency [57].

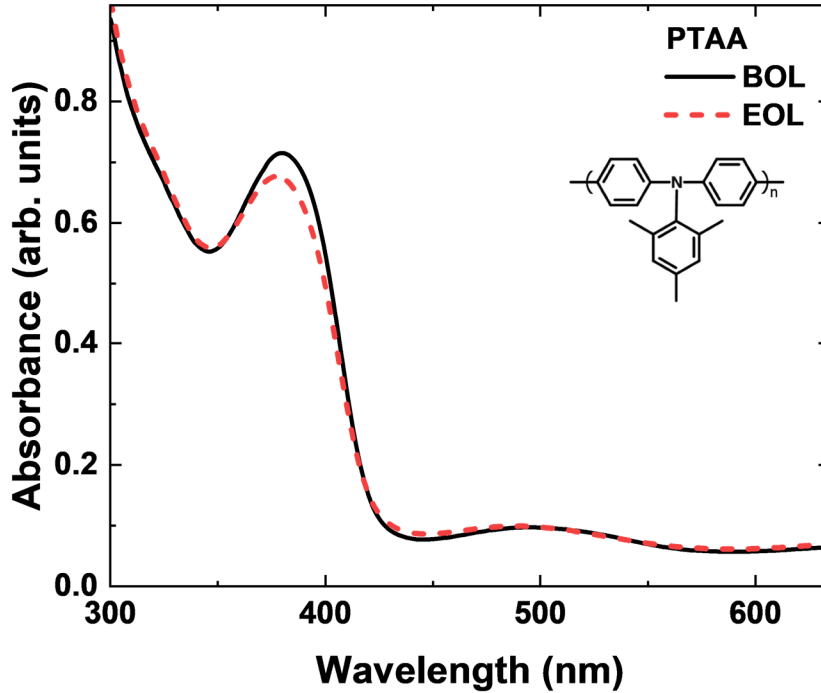


Figure 7. UV-visible Absorbance spectra of PTAA (Stack #5, see Table 2) before and after irradiation at 5×10^{14} protons/cm² @ 1 MeV

It is recalled that in a previous study, J. Barbé *et al.* demonstrated the degradation of Spiro-OMeTAD (HTL) under proton irradiation [58]. While the respective behaviours of spiro-OMeTAD and PTAA have been extensively studied for terrestrial applications [59], to the best of our knowledge, PTAA behaviour under proton irradiation had not been specifically investigated.

4. Electrical characterizations of irradiated & completed sub-part

In order to study the radiation hardness of the Pk and PTAA layer independently, Glass/ITO/SnO₂/Pk (Stack #7, Table 2) and Glass/ITO/SnO₂/Pk/PTAA (Stack #8, Table 2) samples were manufactured. Half of the samples were kept as reference and the other half were irradiated with 5×10^{14} protons/cm² at 1 MeV. Once this step done, all samples (reference & irradiated), were completed so as to measure their PV efficiency. To this end, pristine layers of PTAA and gold electrode were deposited for Stack #7 and pristine layer of gold for Stack #8, respectively.

Figure 8.a shows the *ex-situ* J(V) measurements in AM1.5G of the stack #8 cells. It is clear that the overall electrical properties of the cell are altered after irradiation. One can note a ca 10% decrease in the J_{sc} and the V_{oc} and more importantly a strong increase in series resistance which causes a collapse of the FF (Figure 8). PCE drops by 58% after irradiation of this stack, which is very close to the 52% of degradations observed previously with *in-situ* measurements for the same fluence and energy. Figure 8.b shows the *ex-situ* J(V) measurements under AM1.5G of the cells in stack #7. Conversely, there is almost no difference between the reference cells and the one irradiated up to the Pk layer and then completed with PTAA & gold. Details of the electrical parameter values (PCE, FF, J_{sc} and V_{oc}) and min-max standard

deviations are given in Figure S11. These experiments thus point out that the origin of the observed PSCs performance loss for high protons fluences is not linked to the Pk layer degradation but rather to the PTAA HTL. To further evidence this effect, TLM resistivity measurements were also carried before and after irradiations on Glass ITO/PTAA/Au and Glass ITO/PTAA/ITO_{Top} samples (Stacks #6). Figure S10 shows the increase in contact resistivity after irradiation at 1 MeV 5×10^{14} protons/cm² for both samples types with Au and ITO_{Top} electrodes (from 11.9 to 14.1 mΩ.cm² for gold electrode and from 16.3 to 19.5 mΩ.cm² for ITO electrode). While these stacks do not allow to discriminate between PTAA bulk and interfacial effects, it seems clear that such irradiations lead to significant alteration of PTAA properties.

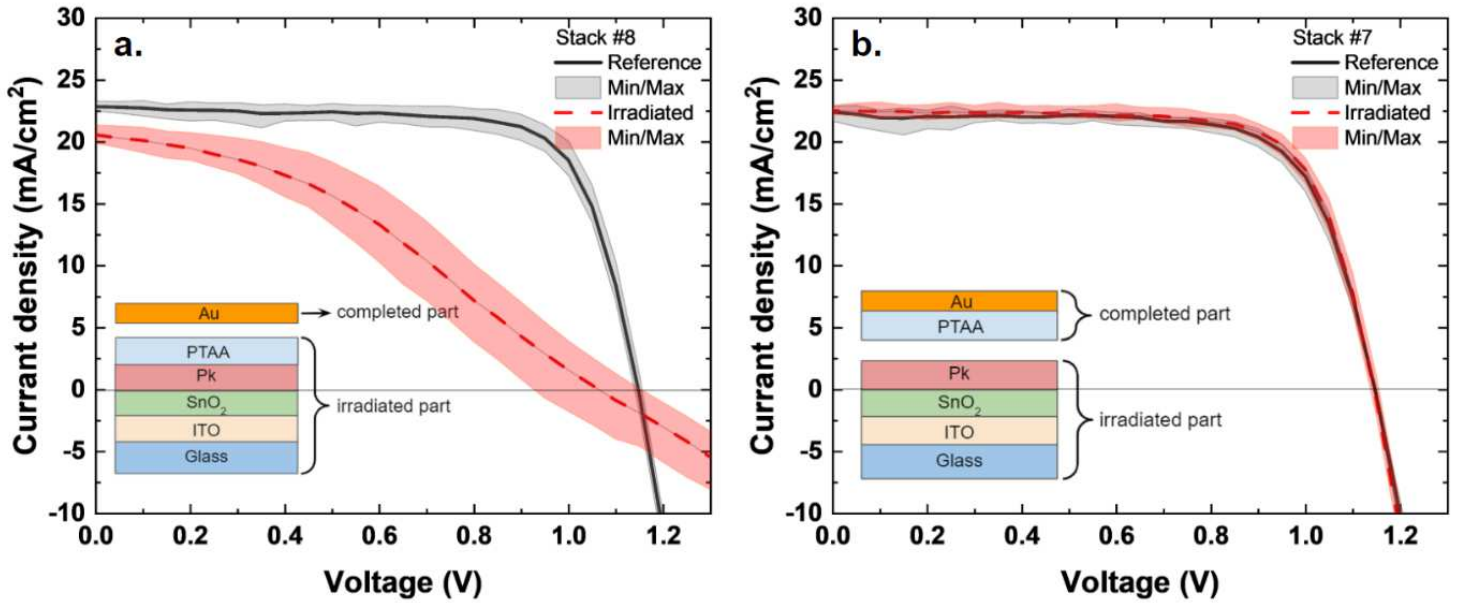


Figure 8. Comparison of $J(V)$ characteristics for PSC before and after $1 \text{ MeV } 5 \times 10^{14} \text{ protons/cm}^2$ irradiation for a. Stack #7 and b. Stack #8 (see Table 2 – error bar refers to min/max data averaged on 6 samples)

Conclusion

In this study, the PSCs radiation hardness under 1 MeV protons irradiations with increasing fluences was analyzed for four different perovskite stoichiometries, using *in-situ* AM0 J(V) measurements. It was found out that for the perovskite with the highest iodine content and lowest bandgap (Eg1 - 1.57 eV) the degradation is more pronounced than the other three series. Moreover, some performance losses during storage (thus without irradiation) has been detected for the large bandgap cells (Eg3 and 4). Thus, the Eg2 = 1.60 eV series (I/Br ratio of 83/17) appeared to be a good compromise between the theoretical AM0 Eg optimum (~ 1.3 eV) and the time stability requirements. This bandgap was thus selected in this study to investigate the irradiation-related degradation mechanisms.

These *in-situ* J(V) measurements also revealed two clear degradations for the PSCs. The first one appears when the samples are exposed to vacuum (without encapsulation) and the second one for an irradiation with a fluence of 5×10^{14} protons/cm². The origin of the device degradation was then investigated using protons irradiations of selected layers constituting the PSCs. From the BOL/EOL characterizations, it appears that the two ITO electrodes (top and bottom), SnO₂ and Pk layers do not show significant electrical, optical nor microstructural degradation at such fluences. On the other hand, the PTAA, the hole transport layer in cells structure, exhibit absorption losses after protons exposure. Such a behaviour could originate from chains scissions of the PTAA molecule that are triggered by the deposited energy, leading to optical degradation and potential electrical properties alteration. This assumption was supported by *ex-situ* J(V) measurements of the electrical properties on cells where PTAA layer had been irradiated and which show pronounced electrical degradation; conversely, the deposition of pristine PTAA layers after Pk irradiation leads to fully performant solar cells, in line with the reference samples. Thus this study demonstrates that irradiation related performance loss of PSCs can be mainly related to the degradation of carriers extraction layers, as seen here with PTAA. The radiation hardness of the Pk absorber layers itself is confirmed with this work (except for high iodine content), underlying at the same time that interfaces and contact layers shall not be neglected for space applications. Future work should thus focus on increasing HTL (and its interfaces) radiation hardness as well as studying the behaviour of the such PSCs and sub-layers under electron irradiations, which are also key constraints in space. More generally, one must be aware that the space environment is full of constraints. This study shows that the perovskite material is well resistant to one of them for a specific architecture and conditions, but many challenges remain to infer the behavior of PSCs in a space environment.

References

- [1] J. M. Raya-Armenta, N. Bazmohammadi, J. C. Vasquez, et J. M. Guerrero, « A short review of radiation-induced degradation of III–V photovoltaic cells for space applications », *Solar Energy Materials and Solar Cells*, vol. 233, p. 111379, déc. 2021, doi: 10.1016/j.solmat.2021.111379.
- [2] W. Guter *et al.*, « Space Solar Cells – 3G30 and Next Generation Radiation Hard Products », *E3S Web Conf.*, vol. 16, p. 03005, 2017, doi: 10.1051/e3sconf/20171603005.
- [3] L. McMillon-Brown, J. M. Luther, et T. J. Peshek, « What Would It Take to Manufacture Perovskite Solar Cells in Space? », *ACS Energy Lett.*, vol. 7, n° 3, p. 1040-1042, mars 2022, doi: 10.1021/acsenergylett.2c00276.
- [4] A. Kojima, K. Teshima, Y. Shirai, et T. Miyasaka, « Organometal Halide Perovskites as Visible-Light Sensitizers for Photovoltaic Cells », *J. Am. Chem. Soc.*, vol. 131, n° 17, p. 6050-6051, mai 2009, doi: 10.1021/ja809598r.
- [5] H. Min *et al.*, « Perovskite solar cells with atomically coherent interlayers on SnO₂ electrodes », *Nature*, vol. 598, n° 7881, Art. n° 7881, oct. 2021, doi: 10.1038/s41586-021-03964-8.
- [6] M. A. Green *et al.*, « Solar cell efficiency tables (Version 60) », *Progress in Photovoltaics: Research and Applications*, vol. 30, n° 7, p. 687-701, 2022, doi: 10.1002/pip.3595.
- [7] M. Shirayama *et al.*, « Degradation mechanism of CH₃NH₃PbI₃ perovskite materials upon exposure to humid air », *Journal of Applied Physics*, vol. 119, n° 11, p. 115501, mars 2016, doi: 10.1063/1.4943638.
- [8] I. Hwang, I. Jeong, J. Lee, M. J. Ko, et K. Yong, « Enhancing Stability of Perovskite Solar Cells to Moisture by the Facile Hydrophobic Passivation », *ACS Appl. Mater. Interfaces*, vol. 7, n° 31, p. 17330-17336, août 2015, doi: 10.1021/acsami.5b04490.
- [9] H.-S. Kim, J.-Y. Seo, et N.-G. Park, « Material and Device Stability in Perovskite Solar Cells », *ChemSusChem*, vol. 9, n° 18, p. 2528-2540, 2016, doi: 10.1002/cssc.201600915.
- [10] A. Bermudez-Garcia, P. Voarino, et O. Raccurt, « Environments, needs and opportunities for future space photovoltaic power generation: A review », *Applied Energy*, vol. 290, p. 116757, mai 2021, doi: 10.1016/j.apenergy.2021.116757.
- [11] Y. Hu *et al.*, « Flexible Perovskite Solar Cells with High Power-Per-Weight: Progress, Application, and Perspectives », *ACS Energy Lett.*, vol. 6, n° 8, p. 2917-2943, août 2021, doi: 10.1021/acsenergylett.1c01193.
- [12] L. Yang *et al.*, « Record-Efficiency Flexible Perovskite Solar Cells Enabled by Multifunctional Organic Ions Interface Passivation », *Advanced Materials*, vol. 34, n° 24, p. 2201681, 2022, doi: 10.1002/adma.202201681.
- [13] N. Jiang *et al.*, « Mechanically and operationally stable flexible inverted perovskite solar cells with 20.32% efficiency by a simple oligomer cross-linking method », *Science Bulletin*, vol. 67, n° 8, p. 794-802, avr. 2022, doi: 10.1016/j.scib.2022.02.010.
- [14] Y. Tu *et al.*, « Perovskite Solar Cells for Space Applications: Progress and Challenges », *Advanced Materials*, vol. 33, n° 21, p. 2006545, 2021, doi: 10.1002/adma.202006545.
- [15] F. Lang *et al.*, « Radiation Hardness and Self-Healing of Perovskite Solar Cells », *Advanced Materials*, vol. 28, n° 39, p. 8726-8731, 2016, doi: 10.1002/adma.201603326.
- [16] S. Kanaya *et al.*, « Proton Irradiation Tolerance of High-Efficiency Perovskite Absorbers for Space Applications », *J. Phys. Chem. Lett.*, vol. 10, n° 22, p. 6990-6995, nov. 2019, doi: 10.1021/acs.jpcllett.9b02665.
- [17] F. Lang *et al.*, « Proton Radiation Hardness of Perovskite Tandem Photovoltaics », *Joule*, vol. 4, n° 5, p. 1054-1069, mai 2020, doi: 10.1016/j.joule.2020.03.006.

- [18] Y. Miyazawa, M. Ikegami, T. Miyasaka, T. Ohshima, M. Imaizumi, et K. Hirose, « Evaluation of radiation tolerance of perovskite solar cell for use in space », in *2015 IEEE 42nd Photovoltaic Specialist Conference (PVSC)*, juin 2015, p. 1-4. doi: 10.1109/PVSC.2015.7355859.
- [19] Z. Song *et al.*, « High Remaining Factors in the Photovoltaic Performance of Perovskite Solar Cells after High-Fluence Electron Beam Irradiations », *J. Phys. Chem. C*, vol. 124, n° 2, p. 1330-1336, janv. 2020, doi: 10.1021/acs.jpcc.9b11483.
- [20] J.-S. Huang *et al.*, « Effects of Electron and Proton Radiation on Perovskite Solar Cells for Space Solar Power Application », in *2017 IEEE 44th Photovoltaic Specialist Conference (PVSC)*, juin 2017, p. 1248-1252. doi: 10.1109/PVSC.2017.8366410.
- [21] I. Cardinaletti *et al.*, « Organic and perovskite solar cells for space applications », *Solar Energy Materials and Solar Cells*, vol. 182, p. 121-127, août 2018, doi: 10.1016/j.solmat.2018.03.024.
- [22] L. K. Reb *et al.*, « Perovskite and Organic Solar Cells on a Rocket Flight », *Joule*, vol. 4, n° 9, p. 1880-1892, sept. 2020, doi: 10.1016/j.joule.2020.07.004.
- [23] W. Delmas *et al.*, « Evaluation of Hybrid Perovskite Prototypes After 10-Month Space Flight on the International Space Station », *Advanced Energy Materials*, vol. n/a, n° n/a, p. 2203920, doi: 10.1002/aenm.202203920.
- [24] G. E. Eperon, M. T. Hörantner, et H. J. Snaith, « Metal halide perovskite tandem and multiple-junction photovoltaics », *Nat Rev Chem*, vol. 1, n° 12, Art. n° 12, nov. 2017, doi: 10.1038/s41570-017-0095.
- [25] M. A. Green, « Limiting photovoltaic efficiency under new ASTM International G173-based reference spectra », *Progress in Photovoltaics: Research and Applications*, vol. 20, n° 8, p. 954-959, 2012, doi: 10.1002/pip.1156.
- [26] D. N. Micha et R. T. Silveiras Junior, « The Influence of Solar Spectrum and Concentration Factor on the Material Choice and the Efficiency of Multijunction Solar Cells », *Sci Rep*, vol. 9, n° 1, Art. n° 1, déc. 2019, doi: 10.1038/s41598-019-56457-0.
- [27] Z. Yang *et al.*, « Stabilized Wide Bandgap Perovskite Solar Cells by Tin Substitution », *Nano Lett.*, vol. 16, n° 12, p. 7739-7747, déc. 2016, doi: 10.1021/acs.nanolett.6b03857.
- [28] S. R. Messenger, G. P. Summers, E. A. Burke, R. J. Walters, et M. A. Xapsos, « Modeling solar cell degradation in space: A comparison of the NRL displacement damage dose and the JPL equivalent fluence approaches† », *Progress in Photovoltaics: Research and Applications*, vol. 9, n° 2, p. 103-121, 2001, doi: 10.1002/pip.357.
- [29] « ECSS-Q-ST-60-15C - Radiation hardness assurance ». Consulté le: 7 décembre 2022. [En ligne]. Disponible sur: <http://everyspec.com/ESA/download.php?spec=ECSS-Q-ST-60-15C.048188.pdf>
- [30] B. K. Durant, H. Afshari, S. Singh, B. Rout, G. E. Eperon, et I. R. Sellers, « Tolerance of Perovskite Solar Cells to Targeted Proton Irradiation and Electronic Ionization Induced Healing », *ACS Energy Lett.*, vol. 6, n° 7, p. 2362-2368, juill. 2021, doi: 10.1021/acsenerylett.1c00756.
- [31] A. R. Kirmani *et al.*, « Countdown to perovskite space launch: Guidelines to performing relevant radiation-hardness experiments », *Joule*, vol. 6, n° 5, p. 1015-1031, mai 2022, doi: 10.1016/j.joule.2022.03.004.
- [32] « ECSS-E-20-08A.pdf ». Disponible sur: https://apc.u-paris.fr/APC_CS/Labo/Espace_Qualite/tch/normes/ECSS/E/ECSS-E-20-08A.pdf
- [33] « SRIM Textbook ». <http://www.srim.org/SRIM%20Book.htm>
- [34] S. Duzellier, G. Hubert, R. Rey, et F. Bezerra, « Mirage: A New Proton Facility for the Study of Direct Ionization in Sub-100nm Technologies », in *2014 IEEE Radiation Effects Data Workshop (REDW)*, juill. 2014, p. 1-5. doi: 10.1109/REDW.2014.7004578.

- [35] S. Duzellier, R. Cariou, T. Nuns, P. Voarino, F. Chabuel, et C. Aicardi, « Benchmark and irradiation tests of terrestrial solar cells for low cost space solar array », in *EU PVSEC 2020*, Lisbonne, Portugal, sept. 2020. doi: hal-02955735.
- [36] J. Tauc, « Optical properties and electronic structure of amorphous Ge and Si », *Materials Research Bulletin*, vol. 3, n° 1, p. 37-46, janv. 1968, doi: 10.1016/0025-5408(68)90023-8.
- [37] M. Rai, L. H. Wong, et L. Etgar, « Effect of Perovskite Thickness on Electroluminescence and Solar Cell Conversion Efficiency », *J. Phys. Chem. Lett.*, vol. 11, n° 19, p. 8189-8194, oct. 2020, doi: 10.1021/acs.jpcclett.0c02363.
- [38] T. Jesper Jacobsson *et al.*, « Exploration of the compositional space for mixed lead halogen perovskites for high efficiency solar cells », *Energy Environ. Sci.*, vol. 9, n° 5, p. 1706-1724, 2016, doi: 10.1039/C6EE00030D.
- [39] N. N. Shlenskaya, N. A. Belich, M. Grätzel, E. A. Goodilin, et A. B. Tarasov, « Light-induced reactivity of gold and hybrid perovskite as a new possible degradation mechanism in perovskite solar cells », *J. Mater. Chem. A*, vol. 6, n° 4, p. 1780-1786, 2018, doi: 10.1039/C7TA10217H.
- [40] D. W. deQuilettes *et al.*, « Photo-induced halide redistribution in organic–inorganic perovskite films », *Nat Commun*, vol. 7, n° 1, Art. n° 1, mai 2016, doi: 10.1038/ncomms11683.
- [41] D. V. Morgan, A. Salehi, Y. H. Aliyu, R. W. Bunce, et D. Diskett, « Radiation damage in indium tin oxide (ITO) layers », *Thin Solid Films*, vol. 258, n° 1-2, p. 283-285, mars 1995, doi: 10.1016/0040-6090(94)06420-2.
- [42] P. Gratia *et al.*, « The Many Faces of Mixed Ion Perovskites: Unraveling and Understanding the Crystallization Process », *ACS Energy Lett.*, vol. 2, n° 12, p. 2686-2693, déc. 2017, doi: 10.1021/acsenerylett.7b00981.
- [43] J. Werner *et al.*, « Sputtered rear electrode with broadband transparency for perovskite solar cells », *Solar Energy Materials and Solar Cells*, vol. 141, p. 407-413, oct. 2015, doi: 10.1016/j.solmat.2015.06.024.
- [44] Y. Jiang *et al.*, « Mitigation of Vacuum and Illumination-Induced Degradation in Perovskite Solar Cells by Structure Engineering », *Joule*, vol. 4, n° 5, p. 1087-1103, mai 2020, doi: 10.1016/j.joule.2020.03.017.
- [45] R. Guo *et al.*, « Degradation mechanisms of perovskite solar cells under vacuum and one atmosphere of nitrogen », *Nat Energy*, vol. 6, n° 10, p. 977-986, oct. 2021, doi: 10.1038/s41560-021-00912-8.
- [46] V. V. Brus *et al.*, « Defect Dynamics in Proton Irradiated CH₃NH₃PbI₃ Perovskite Solar Cells », *Advanced Electronic Materials*, vol. 3, n° 2, p. 1600438, 2017, doi: 10.1002/aelm.201600438.
- [47] C. Besleaga *et al.*, « Iodine Migration and Degradation of Perovskite Solar Cells Enhanced by Metallic Electrodes », *J. Phys. Chem. Lett.*, vol. 7, n° 24, p. 5168-5175, déc. 2016, doi: 10.1021/acs.jpcclett.6b02375.
- [48] C. Li *et al.*, « Iodine Migration and its Effect on Hysteresis in Perovskite Solar Cells », *Advanced Materials*, vol. 28, n° 12, p. 2446-2454, 2016, doi: 10.1002/adma.201503832.
- [49] E. Bi, Z. Song, C. Li, Z. Wu, et Y. Yan, « Mitigating ion migration in perovskite solar cells », *Trends in Chemistry*, vol. 3, n° 7, p. 575-588, juill. 2021, doi: 10.1016/j.trechm.2021.04.004.
- [50] P. Meredith et A. Armin, « Scaling of next generation solution processed organic and perovskite solar cells », *Nat Commun*, vol. 9, n° 1, Art. n° 1, déc. 2018, doi: 10.1038/s41467-018-05514-9.
- [51] D. L. Meier et D. K. Schroder, « Contact resistance: Its measurement and relative importance to power loss in a solar cell », *IEEE Transactions on Electron Devices*, vol. 31, n° 5, p. 647-653, mai 1984, doi: 10.1109/T-ED.1984.21584.

- [52] J. Gierschner, J. Cornil, et H.-J. Egelhaaf, « Optical Bandgaps of π -Conjugated Organic Materials at the Polymer Limit: Experiment and Theory », *Advanced Materials*, vol. 19, n° 2, p. 173-191, 2007, doi: 10.1002/adma.200600277.
- [53] M. Petrović *et al.*, « Limitations of a polymer-based hole transporting layer for application in planar inverted perovskite solar cells », *Nanoscale Adv.*, vol. 1, n° 8, p. 3107-3118, août 2019, doi: 10.1039/C9NA00246D.
- [54] S. A. Nouh, A. Abdel Naby, et P. J. Sellin, « Modification induced by proton irradiation in Makrofol-DE polycarbonate », *Radiation Measurements*, vol. 42, n° 10, p. 1655-1660, nov. 2007, doi: 10.1016/j.radmeas.2007.04.005.
- [55] J.-L. Bonardet et J. Fraissard, *L'indispensable en liaisons chimiques*. Editions Bréal, 2003.
- [56] H. Miyake, R. Uchiyama, et Y. Tanaka, « The relationship between charge accumulation and scission of molecular chain in the proton irradiated PI », in *2016 IEEE International Conference on Dielectrics (ICD)*, juill. 2016, p. 135-138. doi: 10.1109/ICD.2016.7547562.
- [57] N. Yaghoobi Nia, M. Méndez, B. Paci, A. Generosi, A. Di Carlo, et E. Palomares, « Analysis of the Efficiency Losses in Hybrid Perovskite/PTAA Solar Cells with Different Molecular Weights: Morphology versus Kinetics », *ACS Appl. Energy Mater.*, vol. 3, n° 7, p. 6853-6859, juill. 2020, doi: 10.1021/acsaem.0c00956.
- [58] J. Barbé *et al.*, « Radiation Hardness of Perovskite Solar Cells Based on Aluminum-Doped Zinc Oxide Electrode Under Proton Irradiation », *Solar RRL*, vol. 3, n° 12, p. 1900219, 2019, doi: 10.1002/solr.201900219.
- [59] F. M. Rombach, S. A. Haque, et T. J. Macdonald, « Lessons learned from spiro-OMeTAD and PTAA in perovskite solar cells », *Energy Environ. Sci.*, vol. 14, n° 10, p. 5161-5190, 2021, doi: 10.1039/D1EE02095A.

Supporting Information

Perovskite solar cells under protons irradiation: from *in-situ* IV-monitoring to root cause degradation elucidation

Carla Costa^{1,2*}, Matthieu Manceau¹, Sophie Duzellier², Thierry Nuns², Romain Cariou¹
¹Univ. Grenoble Alpes, CEA, Liten, Campus INES, 73375 Le Bourget du Lac, France
²Univ. Toulouse, ONERA, DPHY 31055 Toulouse, France
 *carla.costa@cea.fr

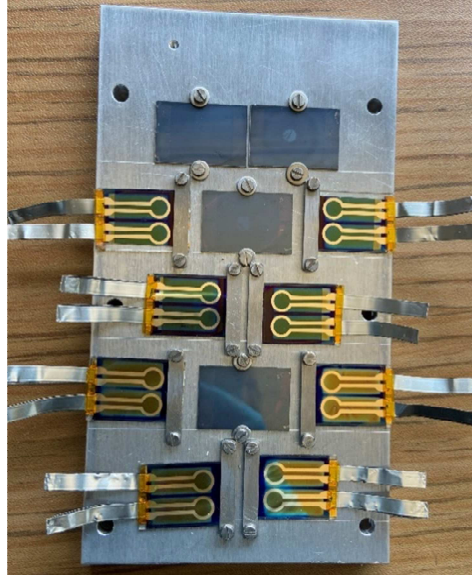


Figure S1: Picture of the sample holder with : 8 substrates positioned so as to be measured under vacuum directly after the irradiations (with two cells per substrate = 16 measurable cells) and 4 places allow irradiation without measurement

Energy used	1 MeV
Total fluence	5×10^{14} protons/cm ²
Average flux	$8,3 \times 10^{10}$ protons/cm ² .s
Average current	13,6 nA
Homogeneity	10 – 15 % on 12 x 12cm ²
Temperature monitoring	25 °C

More details available on publication [34] and on request.

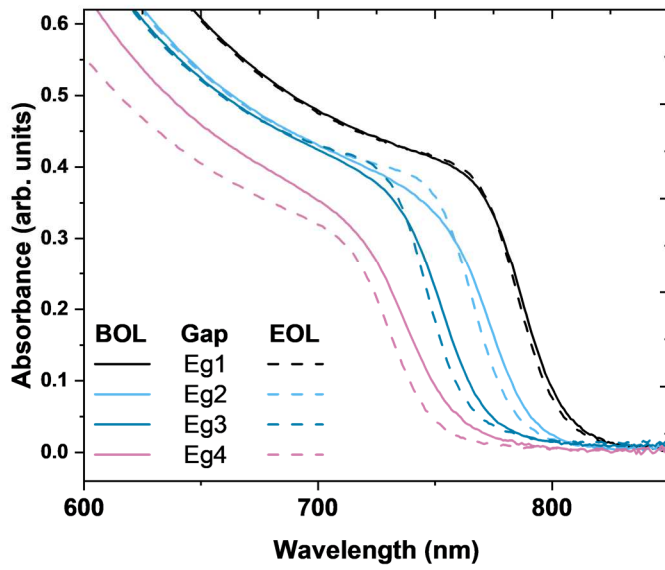


Figure S2. Absorbance spectra Pk material (Stack #1, Table 2) as a function of the bandgap (see Table 1) before and after storage for 7 days in ambient conditions.

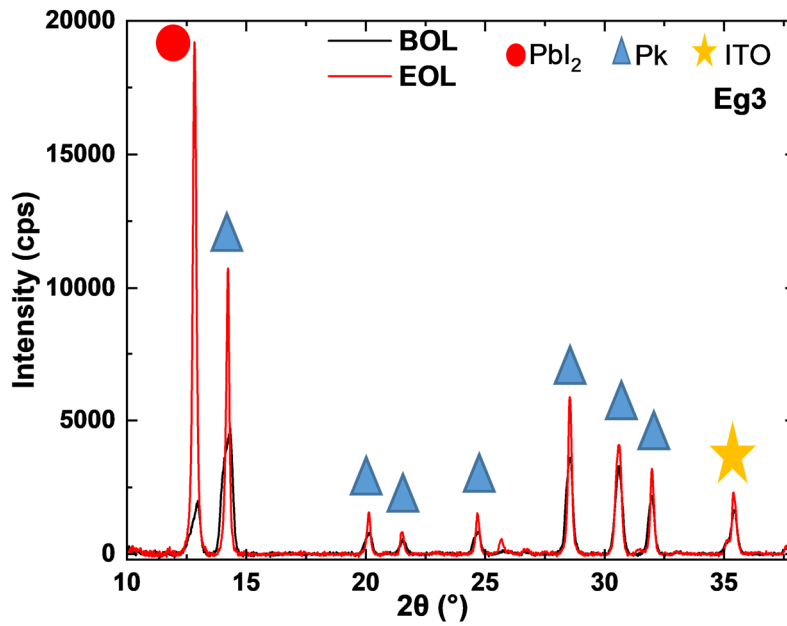


Figure S3. Diffractogram on Glass/ITO/SnO₂/Pk (Stack #1, Table 2) of Eg3, before/after irradiation at 5×10^{14} protons/cm² @ 1MeV

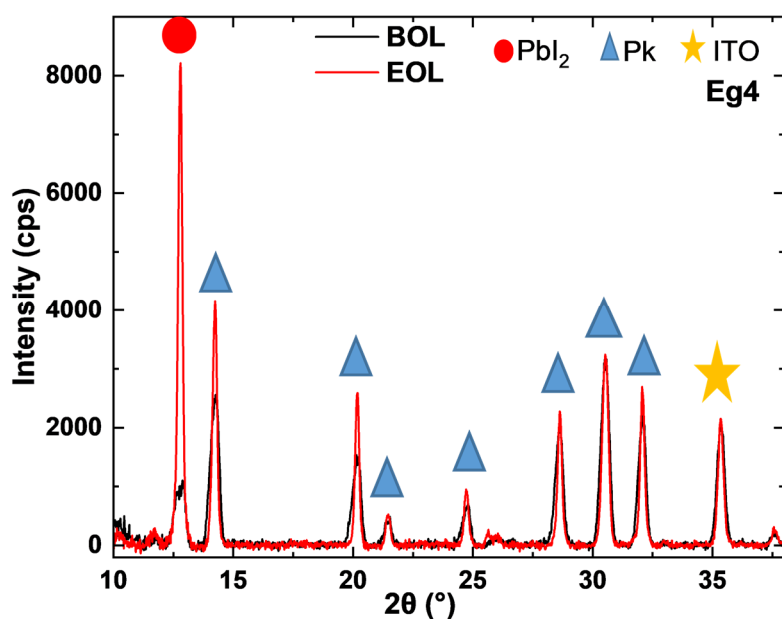


Figure S4. Diffractogram on Glass/ITO/SnO₂/Pk (Stack #1, Table 2) of Eg4, before/after irradiation at 5×10^{14} protons/cm² @1MeV

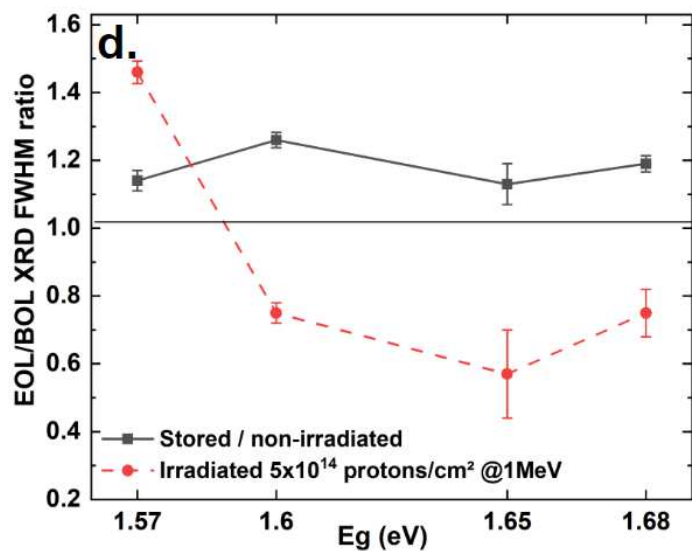


Figure S5 : Evolution of EOL/BOL FWHM as a function of bandgaps (Stack #1, see Table2), for reference samples (solid black line - average of 2 substrates) and after 1 MeV 5×10^{14} protons/cm² (red dash line - average of 4 substrates)

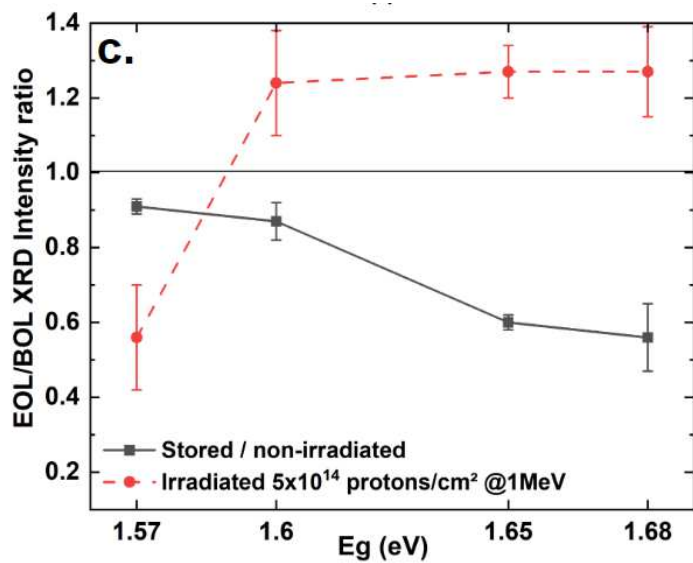


Figure S6: Evolution of EOL/BOL intensity peak (001) as a function of bandgaps (Stack #1, see Table 2), for reference samples (solid black line - average of 2 substrates) and after 1 MeV 5×10^{14} protons/cm² (red dash line - average of 4 substrates)

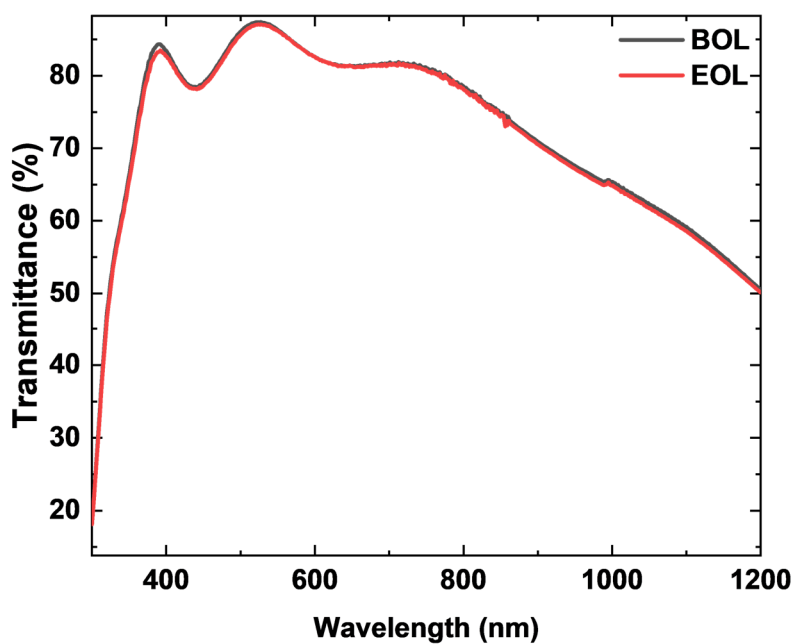


Figure S7. UV/Visible Transmission Spectra of Glass/ITO/SnO₂ (Stack #3, Table 2), before/after irradiation at 5×10^{14} protons/cm² @1MeV

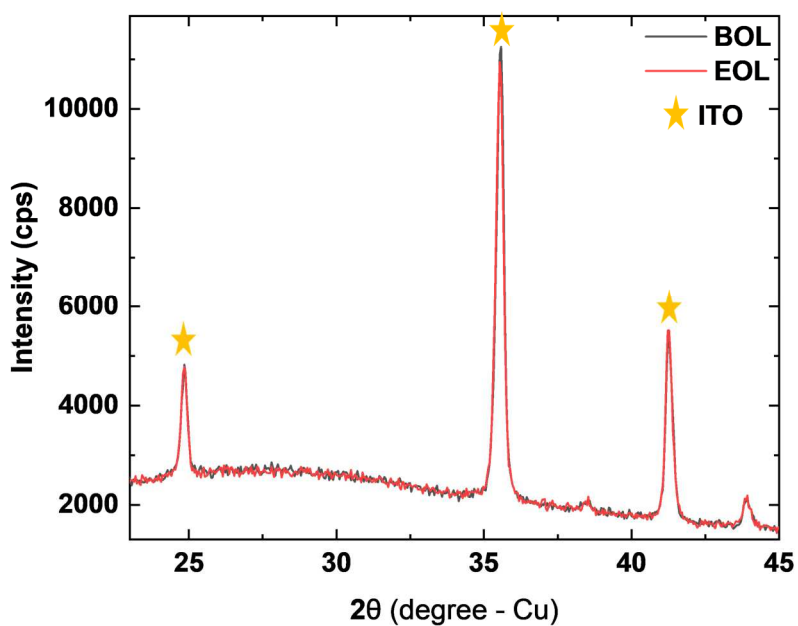


Figure S8. Glass/ITO/SnO₂ XRD patterns (Stack #3, Table 2), before/after irradiation at 5×10^{14} protons/cm² @ 1MeV

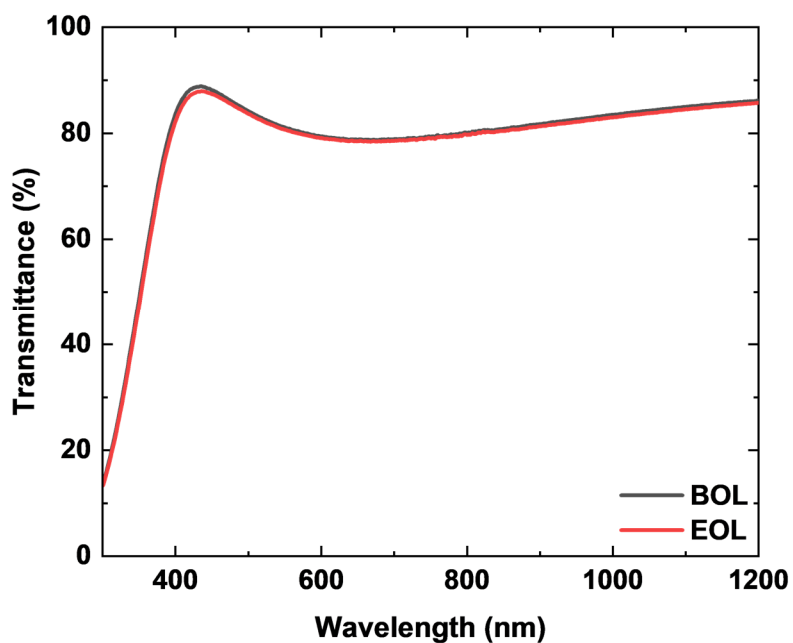


Figure S9. UV/Visible Transmission Spectra of Glass/ITO_{Top} (Stack #4, Table 2), before/after irradiation at 5×10^{14} protons/cm² @ 1MeV

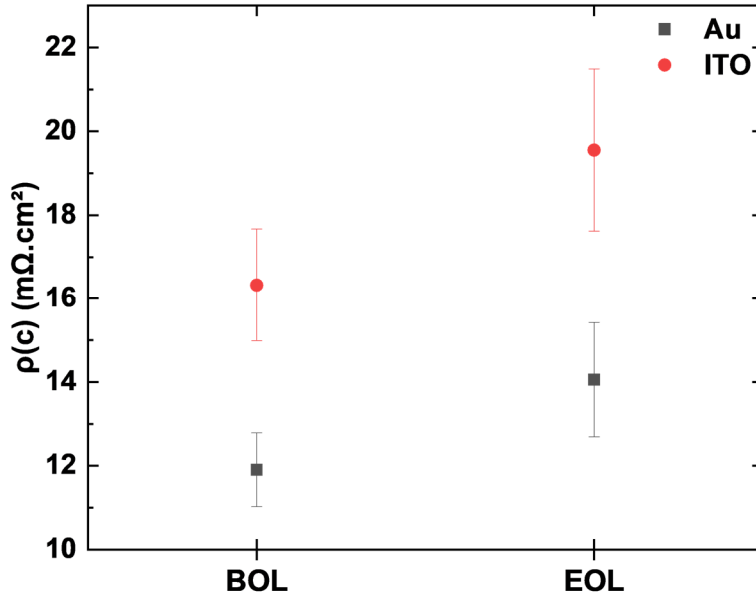


Figure S10. Contact resistivity of Glass/ITO/PTAA/Au (black patterns) and Glass/ITO/PTAA/ITO_{Top} (red patterns) extracted from TLM measurements before/after irradiation at 5×10^{14} protons/cm² @ 1MeV

Stack #8				
Samples	Voc (V)	Jsc (mA/cm ²)	FF (%)	PCE (%)
Reference (non-irradiated)	1.147 +/- 0.004	22.8 +/- 0.3	74 +/- 2	19.4 +/- 0.9
Irradiated	1.063 +/- 0.084	20.5 +/- 0.7	37 +/- 3	8.1 +/- 1.2

Stack #7				
Samples	Voc (V)	Jsc (mA/cm ²)	FF (%)	PCE (%)
Reference (non-irradiated)	1.148 +/- 0.002	22.3 +/- 0.7	72 +/- 1	18.5 +/- 0.7
Irradiated	1.146 +/- 0.006	22.3 +/- 0.7	73 +/- 1	18.7 +/- 0.8

Figure S11. Details of the electrical parameter values (PCE, FF, Jsc and Voc) and min-max standard deviations for Stack #7 and Stack #8.